All-optical nonlinear activation function based on stimulated Brillouin scattering

Grigorii Slinkov[1,*], Steven Becker[1,2,*], Dirk Englund[3], and Birgit Stiller[1,2,†]

[1]Max-Planck-Institute for the Science of Light, Staudtstr. 2, 91058 Erlangen, Germany
[2]Department of Physics, Friedrich-Alexander-Universität Erlangen-Nürnberg, Staudtstr. 7, 91058 Erlangen, Germany
[3]Research Laboratory of Electronics, Massachusetts Institute of Technology, Cambridge, Massachusetts 02139, USA
[*]these authors contributed equally, [†]corresponding author: birgit.stiller@mpl.mpg.de
(Dated: January 11, 2024)

Photonic neural networks have demonstrated their potential over the past decades, but have not yet reached the full extent of their capabilities. One reason for this lies in an essential component – the nonlinear activation function, which ensures that the neural network can perform the required arbitrary nonlinear transformation. The desired all-optical nonlinear activation function is difficult to realize, and as a result, most of the reported photonic neural networks rely on opto-electronic activation functions. Usually, the sacrifices made are the unique advantages of photonics, such as resource-efficient coherent and frequency-multiplexed information encoding. In addition, opto-electronic activation functions normally limit the photonic neural network depth by adding insertion losses. Here, we experimentally demonstrate an in-fiber photonic nonlinear activation function based on stimulated Brillouin scattering. Our design is coherent and frequency selective, making it suitable for multi-frequency neural networks. The optoacoustic activation function can be tuned continuously and all-optically between a variety of activation functions such as LEAKYRELU, SIGMOID, and QUADRATIC. In addition, our design amplifies the input signal with gain as high as 20 dB, compensating for insertion losses on the fly, and thus paving the way for deep optical neural networks.

INTRODUCTION

Artificial neural networks (ANNs) have emerged as powerful instruments for solving difficult tasks that range from speech recognition to image processing in medicine. Thanks to their self-learning abilities and nonlinearity [1], they can provide creative solutions derived from their training on large data sets. After years of rapid scaling of model complexity, machine learning inference and training are close to reaching a bottleneck formed by the limitations of conventional Boolean logic processing hardware, especially with regard to power consumption, latency, and data movement. Overcoming this "von Neumann" bottleneck has motivated the search for new ANN computing architectures based on fundamentally different principles. Transferring the linear algebraic operation – vector-matrix multiplication – of ANNs to the optical domain, in particular, yields a potential for fundamental improvements in energy consumption and latency [2–11]. Although these approaches have demonstrated the potential of optical neural networks (NNs), most of them achieve nonlinearity through opto-electro-optic conversion or digital post-processing [5–10, 12–14]. As the opto-electronic conversion of the signal at each neuron limits the power efficiency, the computing speed, and the scalability of the system [15], all-optical activation functions are demanded [15–18]. The desirable, but so far not demonstrated in one "package", features of an all-optical activation function are: **(i)** programmable nonlinearity, **(ii)** low insertion loss, **(iii)** coherence, **(iv)** frequency selectivity, and **(v)** compatibility with on-chip designs. A programmable activation function allows the optical NN to adapt better to a specific problem and can be used as an additional training parameter. It has been shown for digital NNs that this additional degree of freedom is beneficial for the NN's performance [19, 20]. Insertion losses limit the depth of the neural network, reducing the number of layers that can be stacked before the signal will have to be amplified. A coherent all-optical activation function is not only beneficial for phase-based optical NN architectures, such as [7, 9], but can also allow to implement efficient training schemes [21]. So far, to the best of our knowledge, the only reported coherent activation function is [18]. However, this architecture does not show features **(ii)** and **(iv)** because it attenuates the signal with a saturable-absorber-like response and cannot discriminate between different input frequencies. The latter is an essential of applying resource-efficient frequency-basis information encoding, which is a unique feature of photonics, to optical NNs. Due to the overall lack of a frequency-selective activation function, multi-frequency photonic machine learning architectures have been so far limited to vector-matrix multiplication [10, 22, 23].

Here we experimentally demonstrate an optoacoustic activation function that combines features **(i)**-**(v)** (see Fig. 1). Our design is based on the nonlinear effect of stimulated Brillouin scattering (SBS) [24–26], which arises from the interplay between optical and acoustic fields. Brillouin scattering can be easily observed in optical waveguides, such as optical fibers and on-chip devices [27, 28]. SBS is inherently frequency-selective [29], which makes it particularly suitable for resource-efficient frequency-basis information encoding. This means that our all-optical activation function treats different frequencies independently, while being coherent. Moreover, our approach amplifies the signal with a positive net gain, facilitating its use in deep optical NNs. The nonlinear re-
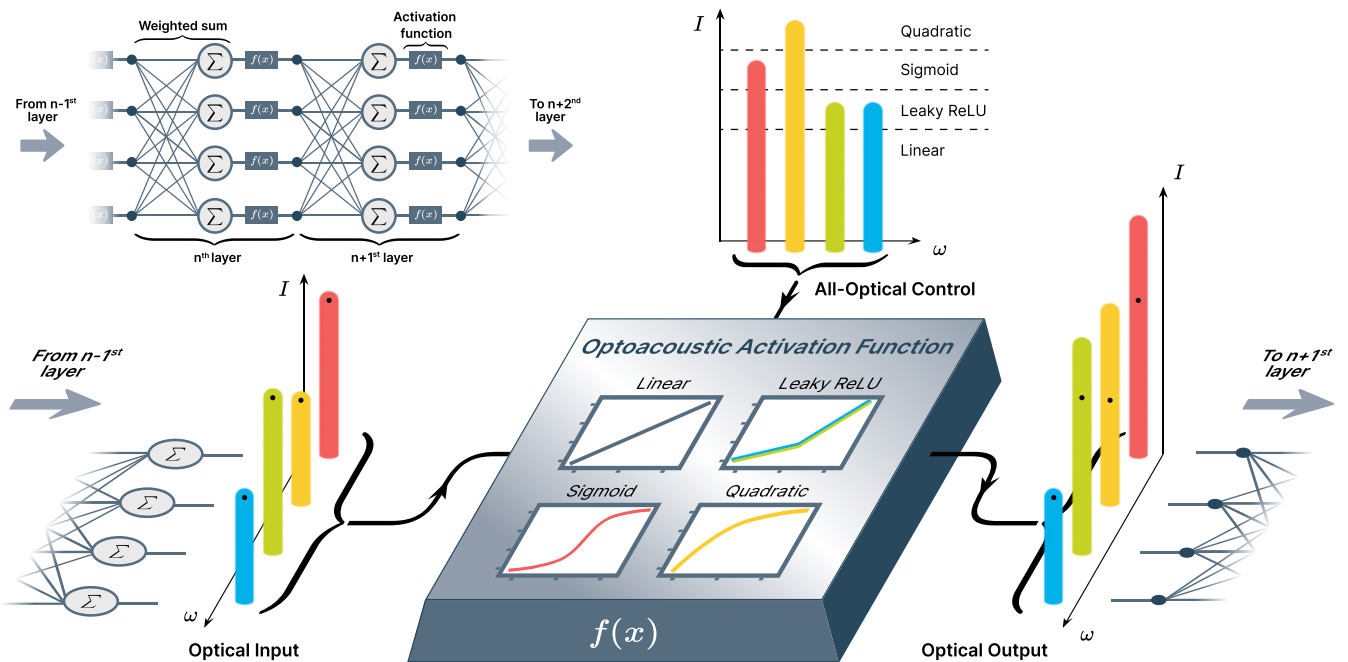
FIG. 1. A schematic representation of an optoacoustic activation function, employed between layers $n-1$ and $n+1$ of an all-optical multi-frequency neural network. The result of the weighted summation of the $n-1^{\text{st}}$ layer is sent to the optoacoustic activation function together with the multi-frequency control signal. The magnitudes of the control signal's spectral components define the type of activation function applied to the corresponding input signal component. The optical output of the optoacoustic activation function has the same frequency components as the input, with their magnitudes nonlinearly transformed depending on the type of activation function. The output is fed to the next layer of the neural network. The inset shows a conceptual scheme of a neural network. Each neuron performs two crucial operations: it takes a weighted sum of the inputs and applies a nonlinear activation function to the result.

sponse is controlled all-optically and can be tuned continuously between different activation function shapes, including LEAKYRELU, SIGMOID and QUADRATIC, which are favored by the machine learning community [5, 20].

While Brillouin scattering has been traditionally used for lasers [30–32], sensing [33, 34], gyroscopes [35, 36], and microscopy [37–39], with our work we reveal new applications, going beyond what has been previously demonstrated for Brillouin-based signal processing [27, 40–45]. Our approach is not limited to a specific platform as SBS can be observed in different waveguide types ranging from optical chips [46–54] and microresonators [55–59] to photonic crystal fiber [41, 60, 61] and fiber tapers [62, 63].

In the following, we demonstrate different nonlinear input-output mappings of the photonic activation function and its tunability. In addition, we apply it to a dual-frequency signal, with a 3 GHz channel separation, demonstrating its frequency selectivity.

I. CONCEPT

Stimulated Brillouin scattering (SBS) is a third-order nonlinear effect that couples a pair of counterpropagating optical waves with a traveling acoustic wave serving as

a mediator between them [24]. It follows a strict phase-matching condition [29]: the frequencies of the optical waves propagating in opposite directions have to be separated by the acoustic wave's frequency Ω, which, for a given optical wavelength, is defined by the properties of the interaction medium. A schematic of an experimental realization is depicted in Figure 2 **a**, where the probe wave a_{probe} is taken to be the one with the lower frequency ω and the pump wave a_{pump} oscillates with the frequency $\omega + \Omega$. The interaction between the fields a_{probe}, a_{pump}, and b can be described formally with the interaction Hamiltonian (1) [64]:

$$\hat{H}_{\text{int}} = \hbar g \int_{-\infty}^{\infty} \mathrm{d}z \left(\hat{a}_{\text{pump}} \, \hat{a}_{\text{probe}}^{\dagger} \, \hat{b}^{\dagger} + \text{H.c.} \right), \quad (1)$$

with the optoacoustic coupling constant g and the time- and space-dependent wave packet operators $\hat{a}_{\text{probe}}(z,t)$, $\hat{a}_{\text{pump}}(z,t)$, $\hat{b}(z,t)$ of the probe, pump and acoustic field, respectively. A detailed description of SBS can be found in the supplementary material.

Our nonlinear activation function is based on a modified Brillouin amplifier scheme that has been demonstrated to deliver high-gain and low-noise operation [65–67]. Under the undepleted pump assumption, the equations governing SBS allow for a simple analytic solution. That is, when the pump is considered to be unaffected
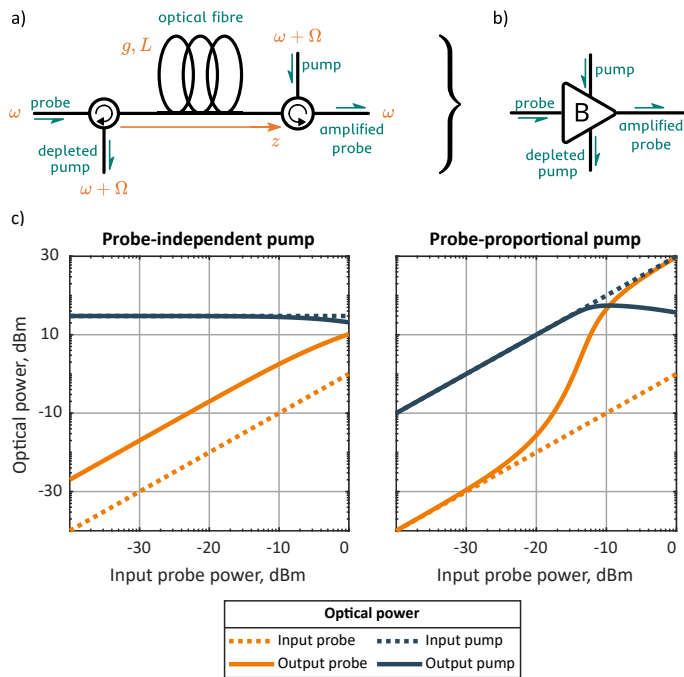
FIG. 2. **a)** A schematic of an optical fibre-based Brillouin amplifier. **b)** A convention introduced to represent the Brillouin amplifier. **c)** Numerical simulation of SBS process, showing linear (left panel) and nonlinear (right panel) relation between the input and the output probe optical power.

by the Brillouin interaction. In this case, the relation between the optical powers of the probe P_{in}, the pump P_{pump} and the amplified probe P_{out} can be written as follows [25, 68]:

$$P_{\mathrm{out}} = P_{\mathrm{in}} \exp(gL \cdot P_{\mathrm{pump}}), \qquad (2)$$

where g is the Brillouin gain and L is the interaction length. We consider now a slightly different situation, where the usually independent pump power is made dependent on the optical input of the Brillouin amplifier: $P_{\mathrm{pump}} = P_{\mathrm{pump}}(P_{\mathrm{in}}) = \gamma P_{\mathrm{in}}$. Then, the Brillouin amplifier shows nonlinear input-output behaviour and equation (2) would write as:

$$P_{\mathrm{out}} = P_{\mathrm{in}} \exp(gL \cdot \gamma P_{\mathrm{in}}) \qquad (3)$$

Solving numerically the corresponding set of coupled mode equations for SBS allows us to study the behaviour of an input-dependent Brillouin amplifier for applying it as a versatile nonlinear activation function for an optical neural network architecture. The corresponding equations can be found in the supplementary material. The simulation results are presented in Fig. 2 **c**. The $g \cdot L$ product is taken to be 0.1 in our simulation. In both panels the input probe power $P_2(0)$ is swept from -40 to 0 dBm. In the left panel the input pump power P_{pump} is kept constant, which results in a linear dependence of probe output P_{out} on the probe input P_{in}. As the output probe power surpasses -10 dBm, the pump starts to

get depleted, and so the probe output growth rate decreases as well. In the right panel both probe P_{in} and pump P_{pump} inputs are swept at the same rate. As one can see, this changes drastically the output probe dynamic: the dependence goes from linear to exponential growth and then back to linear, as we begin to observe the pump depletion. This nonlinear input-output relation in combination with the strict phase matching condition of SBS represents a perfect tool to implement a frequency-selective nonlinear activation function.

II. EXPERIMENTAL RESULTS

A. Single-wavelength operation

The measurement results are presented in Fig. 3, where the output power is plotted against the input power for different 1st stage pump power levels provided by an Erbium-doped fiber amplifier (EDFA). Panel **A** shows a selection of activation function shapes accessible with the setup; panel B demonstrates the complete family of activation function curves. The variation of the EDFA power allows to choose a specific curve, adjusting the activation function shape continuously. When the EDFA is turned off, the activation function is linear.

The selected curves in panel **A** are fitted with analytical activation functions. A pump power of 30.5 dBm corresponds to the LEAKY RELU function. Its first section is a direct proportionality between the input and the output in the absence of SBS process – in this region the pump power is too low to be in the exponential regime of SBS. When the corresponding pump power exceeds the Brillouin threshold, the input light gets amplified. As a result, the input-output dynamic changes its slope as required for LEAKY RELU. The next curve, obtained at pump power of 31.3 dBm, is fitted with SIGMOID. Its nonmonotonic growth can be split into three distinct sections. First, the absence of SBS in the beginning. Second, the amplification provided by SBS in the middle section of the plot. Lastly, the saturated SBS in the final section, where the SBS process becomes so intense that the pump starts to get depleted, resulting in the saturation of the growth. The last curve in Fig.3 **A**, obtained at 32.4 dBm pump power, is fitted with a QUADRATIC function, formed by a SBS process that gives way to saturated SBS as the probe power is increased. The optoacoustic activation function provides a gain of up to 2.4 dB, 8.8 dB, and 21.9 dB for the LEAKY RELU, SIGMOID, and QUADRATIC case, respectively. Hence, the optoacoustic activation function can be used to compensate for losses induced by the preceding matrix operation. This is an essential feature for implementing deep optical NNs.
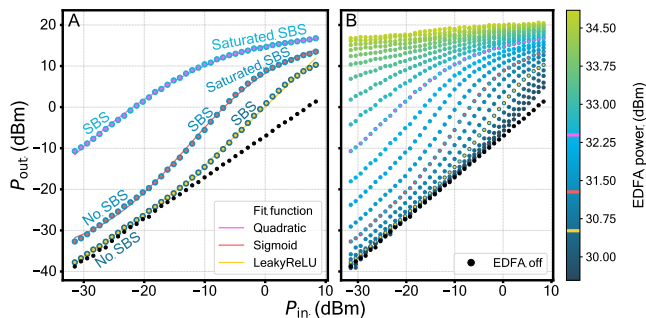
FIG. 3. Nonlinear activation function shapes – the mapping between the optical input and the optical output of the setup. **A** A selection of curves fitted with conventional analytic activation functions. **B** The complete family of curves obtained at various 1$^{\text{st}}$ stage pump optical power levels provided by the EDFA.

B. Dual-wavelength operation

We demonstrate the feature of frequency selectivity by splitting the input into two wavelength-multiplexed channels, provided by two tunable lasers at the input. The frequency separation between the two is set to 3 GHz, limited in the experiment by the spectrum analyzing device resolution.

Each of the two channels hosts its own variable attenuator, which allows us to control the power levels independently (see supplement for details). We use a Finisar WaveAnalyzer to perform a wavelength-selective measurement of optical power at the output. The measurement results are plotted in Fig. 4. Panel **a)** shows the case where the power in channel 1 is swept, while the power in channel 2 is kept constant, panel **b)** is vice versa. In panel **c)** both channels are swept simultaneously. The reference case where both channels are swept, but the EDFA is turned off can be found in the Supplement. The presented selection shows that for a given channel neither the presence, nor the variation of a signal in the neighbouring channel affects the shape of the nonlinear activation function. The SIGMOID activation function shape achieved at maximum EDFA power in the dual-wavelength mode does not match the QUADRATIC shape achieved at maximum EDFA power in the single-wavelength mode. This is due to EDFA distributing its output power equally between the pumps of the two frequency channels, yielding a 3 dB less power per channel.

III. DISCUSSION AND CONCLUSION

We have experimentally demonstrated for the first time, to the best of our knowledge, a nonlinear photonic activation function based on stimulated Brillouin scattering. Our activation function is coherent and frequency selective owing to the nature of SBS. A coherent activation function is the next step from the phase-reliant

optical matrix multiplication approaches [7, 9] to fully all-optical ANNs that would not require opto-electronic conversion, which imposes bandwidth limitations, introduces cross-talk, requires introduction of time delay and eliminates frequency selectivity.

The frequency selectivity opens up prospects of drastically increasing the data throughput by exploiting wavelength multiplexing techniques to, for example, distribute the neurons in a layer across the frequency domain. It is the first demonstration of a frequency sensitive activation function, which shows no correlation between frequency channels that hinders existing solutions, such as frequency-encoded deep neural networks [10]. Moreover, our activation function could transform the existing multi-frequency photonic machine learning architectures (which have been so far limited to linear operations [22, 23]) into actual multi-frequency ANNs. As it has been shown, there is no cross-talk between neighbouring frequency channels at frequency separations as small as 3 GHz, which surpasses the telecommunication standard of 25 GHz. For the continuous wave case, the minimal frequency separation between the two channels is intrinsically limited by the linewidth of the optoacoustic gain function, which, for the commercial single-mode fiber at room temperature is about 26 MHz [69]. As shown in [45, 69], the linewidth can be decreased by lowering the temperature of the waveguide. In the pulsed case, the minimal frequency separation is dictated by the pulse length [29]. The general rule of thumb for SBS-based applications is this: channel separation has to be higher than $\Delta\nu_{\text{laser}} + 1/\tau_{\text{pulse}} + \Delta\nu_{\text{B}}$, where $\Delta\nu_{\text{laser}}$ is the laser linewidth, τ_{pulse} is the pulse length and $\Delta\nu_{\text{B}}$ is the acoustic gain linewidth.

The activation function can be tuned by varying the 1$^{\text{st}}$ Brillouin amplifier's pump power to take such well-proven shapes as LEAKYRELU, SIGMOID, and QUADRATIC. As the dynamics of the 1$^{\text{st}}$ Brillouin amplifier can be controlled externally, it opens the possibility to use the nonlinearity as an additional training parameter of an optical ANN. For digital ANNs, this has been shown to be a powerful tool for boosting the ANN performance [19, 20]. It is also feasible to engineer the 1$^{\text{st}}$ stage pump in such a way that different frequency channels would have different activation function shapes.

The output signal amplification that is inherent to our activation function design is suitable for compensating insertion and propagation losses. This should be particularly useful for designing deep optical NNs that comprise multiple neuron layers [21].

Though the experimental realisation presented in the paper relies on highly nonlinear optical fiber as the optoacoustic interaction medium, our approach is not limited to this platform. Conventional single-mode fiber (SMF) and photonic crystal core fiber (PCF) are also an eligible choice for SBS as well as integrated waveguides, including on-chip devices [27, 43, 70–72]. The choice of the platform combined with pulsed operation constitute the way for improving the energy efficiency of the presented
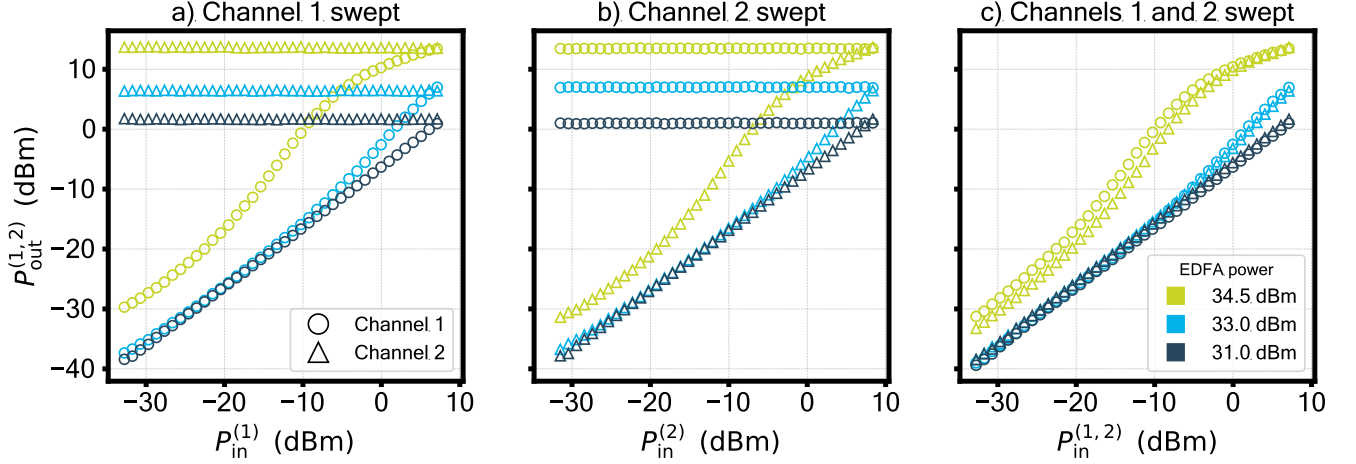
FIG. 4. Demonstration of the frequency-selective operation. Circles and triangles correspond to a pair of wavelength-multiplexed channels, provided by two lasers at the input. The shape of the activation function in either of channels is not affected by the SBS interaction taking place in the neighbouring channel.

optoacoutic activation function. One needs to maximize the term $g \cdot P_{\text{pump}} L_{\text{eff}} - \alpha L$ in order to improve the energy efficiency. Here, P_{pump} is the pump power, L_{eff} is the effective interaction length, and α is the optical loss of the waveguide (see Suppl. for details).

In conclusion, our frequency selective and coherent photonic nonlinear activation fills a gap in the current landscape of photonic machine learning. It could therefore be the key to unlocking the full potential of photonic neuromorphic computing.

IV. METHODS

We implement the photonic nonlinear activation using a setup depicted schematically in Fig. 5. We build what can be called a double-stage Brillouin amplifier: the output of one Brillouin amplifier (1$^{\text{st}}$ stage) is utilized as a pump for another (2$^{\text{nd}}$ stage). The 1$^{\text{st}}$ stage Brillouin amplifier is pumped with an Erbium-doped fiber amplifier (EDFA).

The reason for pumping the 2$^{\text{nd}}$ stage with a Brillouin amplifier, as opposed to applying an EDFA directly, is that conventional EDFAs operate in the saturated regime, providing input-independent output power. This way, replacing the 1$^{\text{st}}$ stage with an EDFA would have eliminated any possible relation between the input and the pump that is required by (3).

The setup is fed with a 1550.12 nm fiber-coupled laser. A voltage-controlled attenuator (VOA) is used in the experiment to test the nonlinear input-output behaviour of the setup, simulating the amplitude-encoded data from the previous neuron layer. The VOA is inserted before the light gets distributed between the two stages, which ensures that they receive the same amplitude variation, as required by (3). Note that feeding the top branch of the setup with the same laser is a measure taken to en-
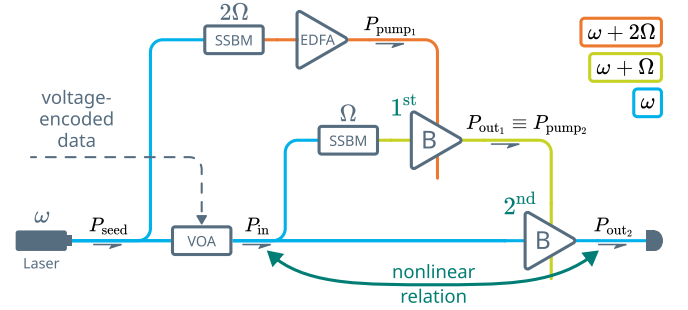

FIG. 5. A principal scheme of the experimental setup: VOA - voltage-operated attenuator, SSBM - single-sideband modulator, EDFA - Erbium-doped fiber amplifier, B - Brillouin amplifier, as introduced in Fig. 2 b. The color of the connecting lines depicts the light frequency.

hance the stability of the Brillouin amplifier and is not an actual requirement.

A Brillouin frequency shift f_{B} (corresponding angular frequency $\Omega = 2\pi f_{\text{B}}$) is applied to the middle branch of the setup, satisfying the SBS phase matching condition for the 2$^{\text{nd}}$ stage. This requires the signal in the top branch to be up-shifted by the sum of the Brillouin frequencies of the fibers. The optical fibre used in both of the stages was of the same material and structure, yielding a 2Ω shift for the top branch.

We use highly nonlinear fiber (HNLF) with equal parameters for the two Brillouin amplifiers. The lengths of the HNLF fibers used for the first and the second stage are 20 m and 100 m, correspondingly. The Brillouin frequency of the fibers is $f_{\text{B}} = 9.730$ GHz. A couple of single sideband modulators (SSBMs) driven with two separate RF sources apply required frequency shifts to the top and the middle branches of the setup.

[1] Oludare Isaac Abiodun, Aman Jantan, Abiodun Esther Omolara, Kemi Victoria Dada, Nachaat AbdElatif Mohamed, and Humaira Arshad. State-of-the-art in artificial neural network applications: A survey. *Heliyon*, 4(11):e00938, November 2018.

[2] Guy Van der Sande, Daniel Brunner, and Miguel C. Soriano. Advances in photonic reservoir computing. *Nanophotonics*, 6(3):561–576, May 2017. Publisher: De Gruyter.

[3] Wim Bogaerts, Daniel Pérez, José Capmany, David A. B. Miller, Joyce Poon, Dirk Englund, Francesco Morichetti, and Andrea Melloni. Programmable photonic circuits. *Nature*, 586(7828):207–216, October 2020. Number: 7828 Publisher: Nature Publishing Group.

[4] Tianwei Wu, Marco Menarini, Zihe Gao, and Liang Feng. Lithography-free reconfigurable integrated photonic processor. *Nature Photonics*, 17(8):710–716, August 2023. Number: 8 Publisher: Nature Publishing Group.

[5] Carlo Michele Valensise, Ivana Grecco, Davide Pierangeli, and Claudio Conti. Large-scale photonic natural language processing, August 2022. arXiv:2208.13649 [physics].

[6] Alexander Sludds, Saumil Bandyopadhyay, Zaijun Chen, Zhizhen Zhong, Jared Cochrane, Liane Bernstein, Darius Bunandar, P. Ben Dixon, Scott A. Hamilton, Matthew Streshinsky, Ari Novack, Tom Baehr-Jones, Michael Hochberg, Manya Ghobadi, Ryan Hamerly, and Dirk Englund. Delocalized photonic deep learning on the internet's edge. *Science*, 378(6617):270–276, October 2022.

[7] Yichen Shen, Nicholas C. Harris, Scott Skirlo, Mihika Prabhu, Tom Baehr-Jones, Michael Hochberg, Xin Sun, Shijie Zhao, Hugo Larochelle, Dirk Englund, and Marin Soljačić. Deep learning with coherent nanophotonic circuits. *Nature Photonics*, 11(7):441–446, July 2017. Number: 7 Publisher: Nature Publishing Group.

[8] Zaijun Chen, Alexander Sludds, Ronald Davis, Ian Christen, Liane Bernstein, Lamia Ateshian, Tobias Heuser, Niels Heermeier, James A. Lott, Stephan Reitzenstein, Ryan Hamerly, and Dirk Englund. Deep learning with coherent VCSEL neural networks. *Nature Photonics*, 17(8):723–730, August 2023.

[9] Saumil Bandyopadhyay, Alexander Sludds, Stefan Krastanov, Ryan Hamerly, Nicholas Harris, Darius Bunandar, Matthew Streshinsky, Michael Hochberg, and Dirk Englund. Single chip photonic deep neural network with accelerated training, August 2022. arXiv:2208.01623 [physics].

[10] Ronald Davis III, Zaijun Chen, Ryan Hamerly, and Dirk Englund. Frequency-Encoded Deep Learning with Speed-of-Light Dominated Latency, July 2022. arXiv:2207.06883 [physics].

[11] Bhavin J. Shastri, Alexander N. Tait, T. Ferreira de Lima, Wolfram H. P. Pernice, Harish Bhaskaran, C. D. Wright, and Paul R. Prucnal. Photonics for artificial intelligence and neuromorphic computing. *Nature Photonics*, 15(2):102–114, February 2021. Number: 2 Publisher: Nature Publishing Group.

[12] Monireh Moayedi Pour Fard, Ian A. D. Williamson, Matthew Edwards, Ke Liu, Sunil Pai, Ben Bartlett, Momchil Minkov, Tyler W. Hughes, Shanhui Fan, and Thien-An Nguyen. Experimental realization of arbitrary activation functions for optical neural networks. *Optics Express*, 28(8):12138, April 2020.

[13] Aashu Jha, Chaoran Huang, and Paul R. Prucnal. Reconfigurable all-optical nonlinear activation functions for neuromorphic photonics. *Optics Letters*, 45(17):4819–4822, September 2020. Publisher: Optica Publishing Group.

[14] Ian A. D. Williamson, Tyler W. Hughes, Momchil Minkov, Ben Bartlett, Sunil Pai, and Shanhui Fan. Reprogrammable Electro-Optic Nonlinear Activation Functions for Optical Neural Networks. *IEEE Journal of Selected Topics in Quantum Electronics*, 26(1):1–12, January 2020.

[15] Mario Miscuglio, Armin Mehrabian, Zibo Hu, Shaimaa I. Azzam, Jonathan George, Alexander V. Kildishev, Matthew Pelton, and Volker J. Sorger. All-optical nonlinear activation function for photonic neural networks [Invited]. *Optical Materials Express*, 8(12):3851, December 2018.

[16] G. Mourgias-Alexandris, A. Tsakyridis, N. Passalis, A. Tefas, K. Vyrsokinos, and N. Pleros. An all-optical neuron with sigmoid activation function. *Optics Express*, 27(7):9620–9630, April 2019. Publisher: Optica Publishing Group.

[17] J. Feldmann, N. Youngblood, C. D. Wright, H. Bhaskaran, and W. H. P. Pernice. All-optical spiking neurosynaptic networks with self-learning capabilities. *Nature*, 569(7755):208–214, May 2019. Number: 7755 Publisher: Nature Publishing Group.

[18] Yang Shi, Junyu Ren, Guanyu Chen, Wei Liu, Chuqi Jin, Xiangyu Guo, Yu Yu, and Xinliang Zhang. Nonlinear germanium-silicon photodiode for activation and monitoring in photonic neuromorphic networks. *Nature Communications*, 13(1):6048, October 2022.

[19] Forest Agostinelli, Matthew Hoffman, Peter Sadowski, and Pierre Baldi. Learning Activation Functions to Improve Deep Neural Networks, April 2015. arXiv:1412.6830 [cs, stat].

[20] Shiv Ram Dubey, Satish Kumar Singh, and Bidyut Baran Chaudhuri. Activation functions in deep learning: A comprehensive survey and benchmark. *Neurocomputing*, 503:92–108, September 2022.

[21] Victor Lopez-Pastor and Florian Marquardt. Self-learning Machines based on Hamiltonian Echo Backpropagation. *Physical Review X*, 13(3):031020, August 2023. arXiv:2103.04992 [nlin, physics:physics].

[22] J. Feldmann, N. Youngblood, M. Karpov, H. Gehring, X. Li, M. Stappers, M. Le Gallo, X. Fu, A. Lukashchuk, A. S. Raja, J. Liu, C. D. Wright, A. Sebastian, T. J. Kippenberg, W. H. P. Pernice, and H. Bhaskaran. Parallel convolutional processing using an integrated photonic tensor core. *Nature*, 589(7840):52–58, January 2021. Number: 7840 Publisher: Nature Publishing Group.

[23] Siddharth Buddhiraju, Avik Dutt, Momchil Minkov, Ian A. D. Williamson, and Shanhui Fan. Arbitrary linear transformations for photons in the frequency synthetic dimension. *Nature Communications*, 12(1):2401, December 2021.

[24] C. Wolff, M. J. A. Smith, B. Stiller, and C. G. Poulton. Brillouin scattering—theory and experiment: tutorial. *Journal of the Optical Society of America B*, 38(4):1243,

April 2021.

[25] Robert W. Boyd. *Nonlinear optics*. Academic Press, Amsterdam ; Boston, 3rd ed edition, 2008.

[26] Andrey Kobyakov, Michael Sauer, and Dipak Chowdhury. Stimulated Brillouin scattering in optical fibers. *Advances in Optics and Photonics*, 2(1):1, March 2010.

[27] Moritz Merklein, Birgit Stiller, Khu Vu, Stephen J. Madden, and Benjamin J. Eggleton. A chip-integrated coherent photonic-phononic memory. *Nature Communications*, 8(1):574, September 2017.

[28] M.O. Van Deventer and A.J. Boot. Polarization properties of stimulated Brillouin scattering in single-mode fibers. *Journal of Lightwave Technology*, 12(4):585–590, April 1994.

[29] Birgit Stiller, Moritz Merklein, Khu Vu, Pan Ma, Stephen J. Madden, Christopher G. Poulton, and Benjamin J. Eggleton. Cross talk-free coherent multi-wavelength Brillouin interaction. *APL Photonics*, 4(4):040802, April 2019.

[30] Sarat Gundavarapu, Grant M. Brodnik, Matthew Puckett, Taran Huffman, Debapam Bose, Ryan Behunin, Jianfeng Wu, Tiequn Qiu, Cátia Pinho, Nitesh Chauhan, Jim Nohava, Peter T. Rakich, Karl D. Nelson, Mary Salit, and Daniel J. Blumenthal. Sub-hertz fundamental linewidth photonic integrated Brillouin laser. *Nature Photonics*, 13(1):60–67, January 2019.

[31] Nils T. Otterstrom, Ryan O. Behunin, Eric A. Kittlaus, Zheng Wang, and Peter T. Rakich. A silicon Brillouin laser. *Science*, 360(6393):1113–1116, June 2018.

[32] Nitesh Chauhan, Andrei Isichenko, Kaikai Liu, Jiawei Wang, Qiancheng Zhao, Ryan O. Behunin, Peter T. Rakich, Andrew M. Jayich, C. Fertig, C. W. Hoyt, and Daniel J. Blumenthal. Visible light photonic integrated Brillouin laser. *Nature Communications*, 12(1):4685, August 2021.

[33] C. A. Galindez-Jamioy and J. M. López-Higuera. Brillouin Distributed Fiber Sensors: An Overview and Applications. *Journal of Sensors*, 2012:1–17, 2012.

[34] Andreas Geilen, Alexandra Popp, Debayan Das, Saher Junaid, Christopher G. Poulton, Mario Chemnitz, Christoph Marquardt, Markus A. Schmidt, and Birgit Stiller. Extreme thermodynamics in nanolitre volumes through stimulated Brillouin–Mandelstam scattering. *Nature Physics*, September 2023.

[35] Jiang Li, Myoung-Gyun Suh, and Kerry Vahala. Microresonator Brillouin gyroscope. *Optica*, 4(3):346, March 2017.

[36] Yu-Hung Lai, Myoung-Gyun Suh, Yu-Kun Lu, Boqiang Shen, Qi-Fan Yang, Heming Wang, Jiang Li, Seung Hoon Lee, Ki Youl Yang, and Kerry Vahala. Earth rotation measured by a chip-scale ring laser gyroscope. *Nature Photonics*, 14(6):345–349, June 2020.

[37] Giuseppe Antonacci, Timon Beck, Alberto Bilenca, Jürgen Czarske, Kareem Elsayad, Jochen Guck, Kyoohyun Kim, Benedikt Krug, Francesca Palombo, Robert Prevedel, and Giuliano Scarcelli. Recent progress and current opinions in brillouin microscopy for life science applications. *Biophysical Reviews*, 12(3):615–624, June 2020.

[38] Robert Prevedel, Alba Diz-Muñoz, Giancarlo Ruocco, and Giuseppe Antonacci. Brillouin microscopy: an emerging tool for mechanobiology. *Nature Methods*, 16(10):969–977, October 2019.

[39] Giuliano Scarcelli and Seok Hyun Yun. Confocal brillouin microscopy for three-dimensional mechanical imaging. *Nature Photonics*, 2(1):39–43, January 2008.

[40] Steven Becker, Dirk Englund, and Birgit Stiller. An optoacoustic field-programmable perceptron for recurrent neural networks, September 2023. arXiv:2309.01543 [physics].

[41] Xinglin Zeng, Philip St.J. Russell, Christian Wolff, Michael H. Frosz, Gordon K. L. Wong, and Birgit Stiller. Nonreciprocal vortex isolator via topology-selective stimulated Brillouin scattering. *Science Advances*, 8(42):eabq6064, October 2022.

[42] David Marpaung, Jianping Yao, and José Capmany. Integrated microwave photonics. *Nature Photonics*, 13(2):80–90, February 2019. Number: 2 Publisher: Nature Publishing Group.

[43] Benjamin J. Eggleton, Christopher G. Poulton, Peter T. Rakich, Michael. J. Steel, and Gaurav Bahl. Brillouin integrated photonics. *Nature Photonics*, 13(10):664–677, October 2019.

[44] Zhaoming Zhu, Daniel J. Gauthier, and Robert W. Boyd. Stored Light in an Optical Fiber via Stimulated Brillouin Scattering. *Science*, 318(5857):1748–1750, December 2007.

[45] Steven Becker, Andreas Geilen, and Birgit Stiller. High-speed coherent photonic random-access memory in long-lasting sound waves, November 2023. arXiv:2311.06219 [physics].

[46] Raphaël Van Laer, Bart Kuyken, Dries Van Thourhout, and Roel Baets. Interaction between light and highly confined hypersound in a silicon photonic nanowire. *Nature Photonics*, 9(3):199–203, March 2015. Number: 3 Publisher: Nature Publishing Group.

[47] Eric A. Kittlaus, Heedeuk Shin, and Peter T. Rakich. Large Brillouin amplification in silicon. *Nature Photonics*, 10(7):463–467, July 2016. Number: 7 Publisher: Nature Publishing Group.

[48] Heedeuk Shin, Jonathan A. Cox, Robert Jarecki, Andrew Starbuck, Zheng Wang, and Peter T. Rakich. Control of coherent information via on-chip photonic–phononic emitter–receivers. *Nature Communications*, 6(1):6427, March 2015. Number: 1 Publisher: Nature Publishing Group.

[49] Moritz Merklein, Birgit Stiller, Khu Vu, Pan Ma, Stephen J. Madden, and Benjamin J. Eggleton. On-chip broadband nonreciprocal light storage. *Nanophotonics*, 10(1):75–82, January 2021. Publisher: De Gruyter.

[50] Dvir Munk, Moshe Katzman, Mirit Hen, Maayan Priel, Moshe Feldberg, Tali Sharabani, Shahar Levy, Arik Bergman, and Avi Zadok. Surface acoustic wave photonic devices in silicon on insulator. *Nature Communications*, 10(1):4214, September 2019. Number: 1 Publisher: Nature Publishing Group.

[51] Flavien Gyger, Junqiu Liu, Fan Yang, Jijun He, Arslan S. Raja, Rui Ning Wang, Sunil A. Bhave, Tobias J. Kippenberg, and Luc Thévenaz. Observation of Stimulated Brillouin Scattering in Silicon Nitride Integrated Waveguides. *Physical Review Letters*, 124(1):013902, January 2020. Publisher: American Physical Society.

[52] Roel Botter, Kaixuan Ye, Yvan Klaver, Radius Suryadharma, Okky Daulay, Gaojian Liu, Jasper van den Hoogen, Lou Kanger, Peter van der Slot, Edwin Klein, Marcel Hoekman, Chris Roeloffzen, Yang Liu, and David Marpaung. Guided-acoustic stimulated Brillouin scattering in silicon nitride photonic circuits. *Science Advances*,

8(40):eabq2196, October 2022. Publisher: American Association for the Advancement of Science.

[53] Kaixuan Ye, Hanke Feng, Yvan Klaver, Akshay Keloth, Akhileshwar Mishra, Cheng Wang, and David Marpaung. Surface acoustic wave stimulated Brillouin scattering in thin-film lithium niobate waveguides, December 2023. arXiv:2311.14697 [physics].

[54] Caique C. Rodrigues, Nick J. Schilder, Roberto O. Zurita, Letícia S. Magalhães, Amirhassan Shams-Ansari, Thiago P. M. Alegre, Marko Lončar, and Gustavo S. Wiederhecker. On-Chip Backward Stimulated Brillouin Scattering in Lithium Niobate Waveguides, November 2023. arXiv:2311.18135 [physics].

[55] Gaurav Bahl, Matthew Tomes, Florian Marquardt, and Tal Carmon. Observation of spontaneous Brillouin cooling. *Nature Physics*, 8(3):203–207, March 2012. Number: 3 Publisher: Nature Publishing Group.

[56] JunHwan Kim, Mark C. Kuzyk, Kewen Han, Hailin Wang, and Gaurav Bahl. Non-reciprocal Brillouin scattering induced transparency. *Nature Physics*, 11(3):275–280, March 2015. Number: 3 Publisher: Nature Publishing Group.

[57] E. A. Cryer-Jenkins, G. Enzian, L. Freisem, N. Moroney, J. J. Price, A. Ø Svela, K. D. Major, and M. R. Vanner. Second-order coherence across the Brillouin lasing threshold. *Optica*, 10(11):1432–1438, November 2023. Publisher: Optica Publishing Group.

[58] G. Enzian, L. Freisem, J.J. Price, A.Ø. Svela, J. Clarke, B. Shajilal, J. Janousek, B.C. Buchler, P.K. Lam, and M.R. Vanner. Non-Gaussian Mechanical Motion via Single and Multiphonon Subtraction from a Thermal State. *Physical Review Letters*, 127(24):243601, December 2021. Publisher: American Physical Society.

[59] G. Enzian, M. Szczykulska, J. Silver, L. Del Bino, S. Zhang, I. A. Walmsley, P. Del'Haye, and M. R. Vanner. Observation of Brillouin optomechanical strong coupling with an 11 GHz mechanical mode. *Optica*, 6(1):7–14, January 2019. Publisher: Optica Publishing Group.

[60] P. Dainese, P. St J. Russell, N. Joly, J. C. Knight, G. S. Wiederhecker, H. L. Fragnito, V. Laude, and A. Khelif. Stimulated Brillouin scattering from multi-GHz-guided acoustic phonons in nanostructured photonic crystal fibres. *Nature Physics*, 2(6):388–392, June 2006. Number: 6 Publisher: Nature Publishing Group.

[61] M. Pang, X. Jiang, W. He, G. K. L. Wong, G. Onishchukov, N. Y. Joly, G. Ahmed, C. R. Menyuk, and P. St J. Russell. Stable subpicosecond soliton fiber laser passively mode-locked by gigahertz acoustic resonance in photonic crystal fiber core. *Optica*, 2(4):339–342, April 2015. Publisher: Optica Publishing Group.

[62] Jean-Charles Beugnot, Sylvie Lebrun, Gilles Pauliat, Hervé Maillotte, Vincent Laude, and Thibaut Sylvestre. Brillouin light scattering from surface acoustic waves in a subwavelength-diameter optical fibre. *Nature Communications*, 5(1):5242, October 2014. Number: 1 Publisher: Nature Publishing Group.

[63] Wendao Xu, Arjun Iyer, Lei Jin, Sze Y. Set, and William H. Renninger. Strong optomechanical interactions with long-lived fundamental acoustic waves. *Optica*, 10(2):206–213, February 2023. Publisher: Optica Publishing Group.

[64] Junyin Zhang, Changlong Zhu, Christian Wolff, and Birgit Stiller. Quantum coherent control in pulsed waveguide optomechanics. *Physical Review Research*, 5(1):013010, January 2023.

[65] C. N. Pannell, P. St J. Russell, and T. P. Newson. Stimulated Brillouin scattering in optical fibers: the effects of optical amplification. *JOSA B*, 10(4):684–690, April 1993. Publisher: Optica Publishing Group.

[66] Liang Xing, Li Zhan, Shouyu Luo, and Yuxing Xia. High-Power Low-Noise Fiber Brillouin Amplifier for Tunable Slow-Light Delay Buffer. *IEEE Journal of Quantum Electronics*, 44(12):1133–1138, December 2008.

[67] Mark Pelusi, Takashi Inoue, and Shu Namiki. Brillouin Amplifier Noise Characterization by a Coherent Receiver and Digital Signal Processing. *Journal of Lightwave Technology*, 38(16):4221–4236, August 2020.

[68] Fikri Serdar Gökhan, Hasan Göktaş, and Volker J. Sorger. Analytical approach of Brillouin amplification over threshold. *Applied Optics*, 57(4):607, February 2018.

[69] S. Le Floch and P. Cambon. Study of Brillouin gain spectrum in standard single-mode optical fiber at low temperatures (1.4–370 K) and high hydrostatic pressures (1–250 bars). *Optics Communications*, 219(1-6):395–410, April 2003.

[70] Amol Choudhary, Blair Morrison, Iman Aryanfar, Shayan Shahnia, Mattia Pagani, Yang Liu, Khu Vu, Stephen Madden, David Marpaung, and Benjamin J. Eggleton. Advanced Integrated Microwave Signal Processing With Giant On-Chip Brillouin Gain. *Journal of Lightwave Technology*, 35(4):846–854, February 2017.

[71] Laura Blázquez Martínez, Philipp Wiedemann, Changlong Zhu, Andreas Geilen, and Birgit Stiller. Optoacoustic cooling of traveling hypersound waves, May 2023. arXiv:2305.19823 [physics, physics:quant-ph].

[72] Blair Morrison, Alvaro Casas-Bedoya, Guanghui Ren, Khu Vu, Yang Liu, Atiyeh Zarifi, Thach G. Nguyen, Duk-Yong Choi, David Marpaung, Stephen J. Madden, Arnan Mitchell, and Benjamin J. Eggleton. Compact Brillouin devices through hybrid integration on silicon. *Optica*, 4(8):847, August 2017.

Supplementary information: All-optical nonlinear activation function based on stimulated Brillouin scattering

Grigorii Slinkov[1,*], Steven Becker[1,2,*], Dirk Englund[3], and Birgit Stiller[1,2,†]

[1]Max-Planck-Institute for the Science of Light, Staudtstr. 2, 91058 Erlangen, Germany
[2]Department of Physics, Friedrich-Alexander-Universität Erlangen-Nürnberg, Staudtstr. 7, 91058 Erlangen, Germany
[3]Research Laboratory of Electronics, Massachusetts Institute of Technology, Cambridge, Massachusetts 02139, USA
[*]these authors contributed equally, [†]corresponding author: birgit.stiller@mpl.mpg.de
(Dated: January 11, 2024)

This document provides supplementary information to "All-optical nonlinear activation function based on stimulated Brillouin scattering". Detailed description of the stimulated Brillouin scattering effect, extended description of the experimental setup, details on energy efficiency and latency of the nonlinear activation function are presented.

I. DETAILED DESCRIPTION OF BRILLOUIN SCATTERING

In the following, we describe the underlying dynamic of stimulated Brillouin scattering (SBS) using Figure S1. A more detailed description can be found in References [1–4]. The coincidence of the two counter-propagating op-
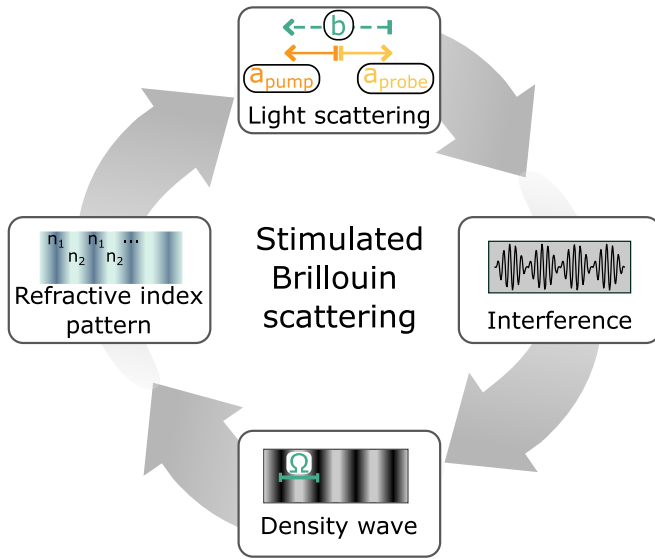

FIG. S1. Illustrated of the SBS feedback mechanism Initially, light waves ω_{probe} and a_{pump} scatter off acoustic phonons b, experiencing a frequency shift known as Brillouin frequency Ω. The interplay between the incident and backscattered light fields generates a dynamic interference pattern in motion. Electrosriction then translates this pattern into a mobile density wave, changing the refractive index n of the medium due to the photoelastic effect. This resulting density wave augments scattering efficiency, enabling a stimulated process.

tical fields a_{probe} at frequency ω_{probe} and a_{pump} at frequency $\omega_{\mathrm{pump}} = \omega_{\mathrm{probe}} + \Omega$ in the waveguide creates an interference pattern. Through the effect of electrostriction, the interference pattern excites a traveling acoustic wave b. As the density variation is connected to the optical refractive index n of the medium, the optical waves

are thus exposed to a moving Bragg-grating-like refractive index pattern. This causes an inelastic scattering of the a_{pump} into the probe wave a_{probe} and the acoustic wave b which then enhances the interference, substantiating the stimulated nature of the process.

II. EXTENDED ILLUSTRATION OF THE EXPERIMENTAL SETUP

The extended experimental setup used for both the single and dual-frequency study is shown in Figure S2. The setup is fed with a pair of lasers to simulate the frequency-multiplexed input. The separation between the two frequency channels $\omega_1 - \omega_2 \approx 3\,\mathrm{GHz}$ is set by tuning the individual wavelengths of the lasers. For the single-wavelength study the setup was the same, but only one of the two lasers was used.

Each laser's output is split using a 50:50 coupler. One half is then used for the nonlinear activation function, whereas the other serves as a seed for the optical pump branch. The input power of the nonlinear activation function is controlled by a voltage-operated attenuator (VOA). In the dual-frequency experiment a second VOA is used for each of the two lasers, ensuring independent control of optical power for each of the frequency channels. The two frequency channels are combined using a 50:50 coupler. Their combination forms the activation function input, which will undergo the desired nonlinear transformation. The coupler acts also as splitter, feeding its input to the bottom and the middle branches of the setup which constitute the nonlinear activation function.

The (dual-frequency) signal in the lower branch serves as the input for the 2nd stage Brillouin amplifier based on a 100 m long highly nonlinear fiber (HNLF).

The (dual-frequency) signal in the middle branch is first up-shifted by the Brillouin frequency of the HNLF $f_{\mathrm{B}} = 9.730\,\mathrm{GHz}$ (corresponding angular frequency $\Omega = 2\pi f_{\mathrm{B}}$) with an optical IQ-modulator, which is configured to operate as a single-sideband modulator (SSBM). The resulting frequency up-shifted signal gets amplified by the 1st stage Brillouin amplifier based on a 20 m long
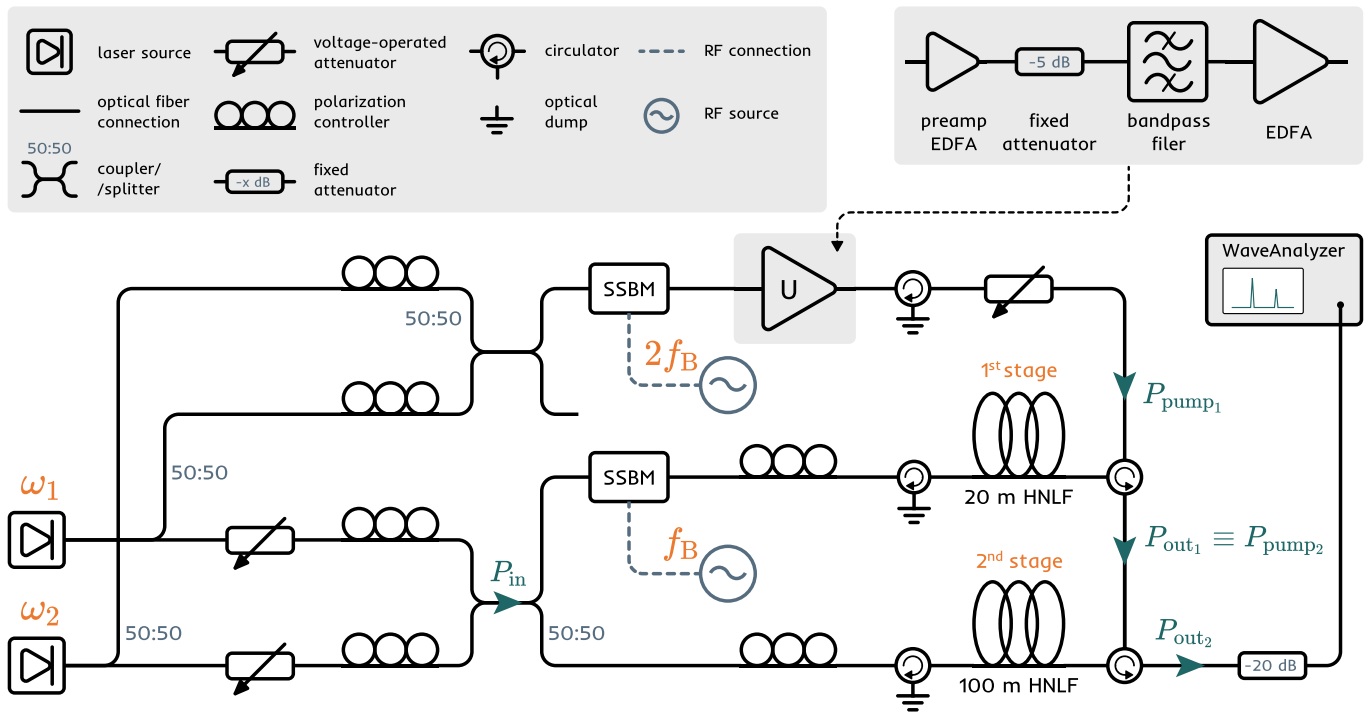
FIG. S2. Extended illustration of the experimental setup used in the study. In the single-frequency case one of the lasers was turned off.

HNLF. After that, it serves as the pump for the 2nd stage Brillouin amplifier.

The top branch of the setup provides the optical pump for the 1st stage Brillouin amplifier. Thus, it is seeded with the original laser combination, up-shifted by twice the Brillouin frequency and amplified by two cascaded Erbium-doped fiber amplifiers (EDFA). The first one acts as a pre-amplifier to seed the second high-power EDFA. Between the two EDFAs we apply a fixed value attenuator to comply with the input power limitations of the high-power EDFA. It is followed by a 1 nm bandpass filter to reduce the amplified spontaneous noise (ASE) level. A circulator isolates the EDFA from possible light backreflection and could be replaced with an optical isolator. The output power of the top branch is controlled with a third VOA for precise and quick tuning.

The output of the second Brillouin amplifier (2nd stage) forms the output of the nonlinear activation function. It is detected with a WaveAnalyzer [5] that performs a frequency-selective measurement.

III. DUAL CHANNEL INPUT-OUTPUT REFERENCE

Figure S3 shows linear input-output dynamic for both frequency-multiplexed channels when the EDFA is turned off. It provides a reference for the Figure 4 of the manuscript. Power in both channels is swept.
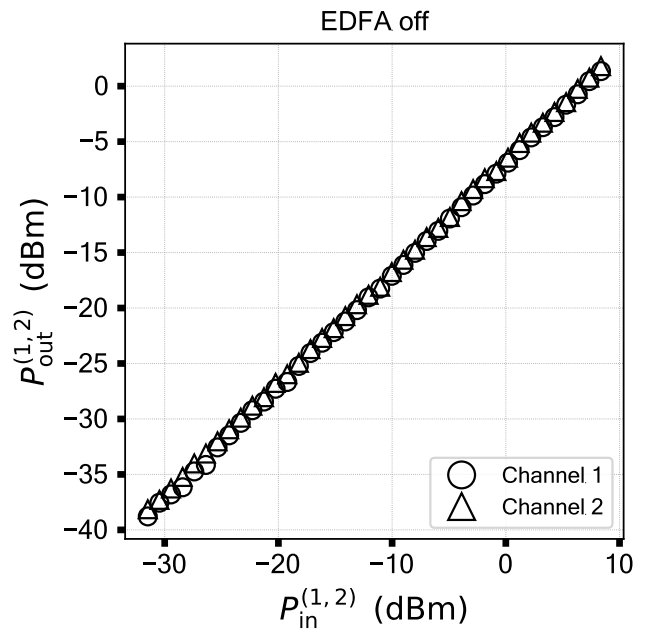

FIG. S3. Dual-frequency operation with the EDFA turned off.

IV.   NUMERICAL STUDY DETAILS

In a unidimensional waveguide (optical fibre) the equations governing SBS process can be written in terms of pump and probe optical power. Although these equations allow for an analytical solution [6], we follow the numerical approach discussed in [2]. We solve the set of equations (S.1) in the conservative limit (no absorption):

$$\begin{cases} \frac{\partial P_1}{\partial z} = -gP_1P_2 \\ \frac{\partial P_2}{\partial z} = -gP_1P_2, \end{cases} \qquad (S.1)$$

where $P_1 = P_1(z)$ and $P_2 = P_2(z)$ are the pump and the probe power measured along the fiber length z (Fig. S4), correspondingly, which means that following the conventions introduced in Section I of the main text,

$$\begin{cases} P_1(L) = P_{\text{pump}} \\ P_2(0) = P_{\text{in}} \end{cases} \qquad (S.2)$$

Fig. 2 **c** of the main text presents the results of solving (S.1) with boundary conditions (S.2).

V.   ENERGY-EFFICIENCY

In order to reduce the power required to pump the first Brillouin amplifier and therefore enhance the overall energy efficiency of the activation function, one can choose a longer waveguide with higher optoacoustic gain g.

Firstly, this will reduce the minimum pump power required to transfer from the spontaneous to the stimulated regime which can be approximately with Equation (S.3) [4].

$$P_{\text{th}} = \frac{21K}{gL_{\text{eff}}}, \qquad (S.3)$$

with the effective interaction length $L_{\text{eff}} = (1 - \exp(-\alpha L))/\alpha$, the optical loss α, the effect of copolarized light $K = 3/2$ [7], and the peak Brillouin gain g. In our case, we can assume $\alpha_{\text{HNLF}} = 0.28\,\text{km}^{-1}$, $g_{\text{HNLF}} = 1.25\,\text{W}^{-1}\,\text{m}^{-1}$ [8], which yields $P_{\text{th}} = 1.26\,\text{W}$ and $P_{\text{th}} = 256\,\text{mW}$ for the first and the second Brillouin amplifier, respectively.

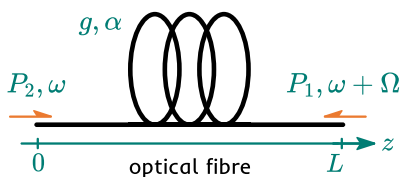Secondly, a higher gain length product will reduce the amount of pump power to achieve similar gain values as demonstrated. In the simplest case, the gain of a Brillouin amplifier can be written as in Equation (S.4).

$$g_{\text{amp}} = \exp(gL_{\text{eff}}P_{\text{pump}} - \alpha L) \qquad (S.4)$$

with the intrinsic Brillouin gain g and the waveguide length L. Accordingly, the pump power P_{pump} can be reduced by increasing the Brillouin gain g and L_{eff}, which could be achieved with chalcogenide waveguides such as rib chips and fibers or photonic crystal fibers [9, 10].

The current HNLF-based design with the first Brillouin amplifier length $L = 20\,\text{m}$ offers $10\log_{10}(g_{\text{amp}}) \approx 54\,\text{dB}$ gain driven with $P_{\text{pump}} = 500\,\text{mW}$. In a chalcogenide waveguide, given the experimentally demonstrated parameters $g_{\text{AsS}} = 500\,\text{W}^{-1}\,\text{m}^{-1}$, $\alpha_{\text{AsS}} = 1.2\,\text{km}^{-1}$ and chip length of $L_{\text{AsS}} = 0.2\,\text{m}$ [9, 11], the same gain can be achieved with $80\,\%$ less pump power required: $P_{\text{pump,AsS}} \approx 0.12\,\text{W}$. Note that even chip designs with $g_{\text{AsS}} = 750\,\text{W}^{-1}\,\text{m}^{-1}$ have been shown experimentally, however with a shorter waveguide length [12].

VI.   LATENCY OF THE OPTOACOUSTIC ACTIVATION FUNCTION

The latency of the optoacoustic nonlinear activation function is dictated by the time of flight τ of the the 2$^{\text{nd}}$ stage Brillouin amplifier. Assuming that this device has the length $L_{\text{NLA}} = L_{\text{waveguide}} + L_{\text{components}}$ which is written as the sum of the legnth of the SBS-active waveguide $L_{\text{waveguide}}$, such as the HNLF, and the length of the components $L_{\text{components}}$ which feed the light into the waveguide and out - for instance, the circulators. Then the ToF can be written as Equation (S.5).

$$\tau_{\text{NLA}} = L_{\text{NLA}}n_{\text{eff}}/c_0 \qquad (S.5)$$

with the effective refractive index of the waveguide n_{eff} and the speed of light c_0. For the nonlinear activation function used in our study assuming $L_{\text{NLA,HNLF}} \approx 108\,\text{m}$ and $n_{\text{eff}} = 1.44$ yields a latency of $\tau_{\text{NLA,HNLF}} \approx 500\,\text{ns}$.

FIG. S4. Brillouin process in an optical fiber. P_2 is the probe wave, P_1 is the pump wave.

[1] C. Wolff, M. J. A. Smith, B. Stiller, and C. G. Poulton. Brillouin scattering—theory and experiment: tutorial. *Journal of the Optical Society of America B*, 38(4):1243, April 2021.

[2] Robert W. Boyd. *Nonlinear optics*. Academic Press, Amsterdam ; Boston, 3rd ed edition, 2008.

[3] Andrey Kobyakov, Michael Sauer, and Dipak Chowdhury. Stimulated Brillouin scattering in optical fibers. *Advances in Optics and Photonics*, 2(1):1, March 2010.

[4] Govind Agrawal. Stimulated Brillouin Scattering. In *Nonlinear Fiber Optics*, pages 353–396. Elsevier, 2013.

[5] WaveAnalyzer 1500S High-Resolution Optical Spectrum Analyzer | Coherent Corp.

[6] Fikri Serdar Gökhan, Hasan Göktaş, and Volker J. Sorger. Analytical approach of Brillouin amplification over threshold. *Applied Optics*, 57(4):607, February 2018.

[7] M.O. Van Deventer and A.J. Boot. Polarization properties of stimulated Brillouin scattering in single-mode fibers. *Journal of Lightwave Technology*, 12(4):585–590, April 1994.

[8] Steven Becker, Andreas Geilen, and Birgit Stiller. High-speed coherent photonic random-access memory in long-lasting sound waves, November 2023. arXiv:2311.06219 [physics].

[9] Benjamin J. Eggleton, Christopher G. Poulton, Peter T. Rakich, Michael. J. Steel, and Gaurav Bahl. Brillouin integrated photonics. *Nature Photonics*, 13(10):664–677, October 2019.

[10] Laura Blázquez Martínez, Philipp Wiedemann, Changlong Zhu, Andreas Geilen, and Birgit Stiller. Optoacoustic cooling of traveling hypersound waves, May 2023. arXiv:2305.19823 [physics, physics:quant-ph].

[11] Amol Choudhary, Blair Morrison, Iman Aryanfar, Shayan Shahnia, Mattia Pagani, Yang Liu, Khu Vu, Stephen Madden, David Marpaung, and Benjamin J. Eggleton. Advanced Integrated Microwave Signal Processing With Giant On-Chip Brillouin Gain. *Journal of Lightwave Technology*, 35(4):846–854, February 2017.

[12] Blair Morrison, Alvaro Casas-Bedoya, Guanghui Ren, Khu Vu, Yang Liu, Atiyeh Zarifi, Thach G. Nguyen, Duk-Yong Choi, David Marpaung, Stephen J. Madden, Arnan Mitchell, and Benjamin J. Eggleton. Compact Brillouin devices through hybrid integration on silicon. *Optica*, 4(8):847, August 2017.